

## STICK-SLIP PATTERNS IN COUPLED EXTENSIONAL/TORSIONAL VIBRATIONS OF DRILL-STRINGS

Rubens Sampaio\*, Marcelo T. Piovan\*<sup>†</sup>, and Germaín Venero Lozano\*

\*Departamento de Engenharia Mecânica  
Pontifícia Universidad Católica - Rio de Janeiro,  
Marquês de São Vicente 225 (22453-900) Gávea, Rio de Janeiro, Brasil  
email: (rsampaio,mpiovan,gvenero)@mec.puc-rio.br, web page: <http://www.mec.puc-rio.br>

<sup>†</sup>Grupo Análisis de Sistemas Mecánicos  
Universidad Tecnológica Nacional Facultad Regional Bahía Blanca,  
11 de Abril 461 (B8000LMI), Bahía Blanca, Argentina  
email: [mpiovan@frbb.utn.edu.ar](mailto:mpiovan@frbb.utn.edu.ar), web page: <http://www.frbb.utn.edu.ar/gasm>

**Key Words:** drill-string, non-linear dynamics, axial/torsional, finite elements, stick-slip.

**Abstract.** *In the present work a geometrically non-linear model is presented to study the coupling of axial and torsional vibrations on a drill-string, which is described as a vertical slender beam under axial rotation. The beam is subjected to distributed loads due to its own weight and the reaction forces at the lower end. It is known that the geometrical nonlinearities play an important role in the stiffening of a beam. The objective of this work is to understand the geometrical stiffening/softening effects of axial-torsional coupled vibrations of drill-strings in different operative conditions. Here, the geometrical stiffening is analyzed using a non-linear finite element approximation, in which large rotations and nonlinear strain-displacements are taken into account. The effect of structural damping is also included in the model. To help to understand these effects comparisons of the present model with linear ones were simulated and time responses and operative variables were compared. The analysis shows that linear and non-linear models differ considerably after the first periods of stick-slip. The behavior is more evident with the increase of the friction process in the lower part of the drill. One of the main differences between the models is that the linear model predicts higher rotary speed peaks -in a stick-slip situation- than the non-linear.*

## 1 INTRODUCTION

It is well known that flexible beams subjected to axial loads manifest stiffness variations, due to the presence of the geometric stiffening effect,<sup>1</sup> which is inherently non-linear. The problem of geometrical stiffening in the context of dynamics of structures was analyzed by means of different schemes such as those reported in the works of Banerjee and Dickens<sup>2</sup> and Trindade and Sampaio.<sup>3</sup> The non-linear effects are relevant in the case of drill-strings vibrations and it deserves some attention in order to develop suitable models, as it was advanced by Trindade, Wolter and Sampaio.<sup>4</sup> Vibrations of drill-strings are often analyzed by means of discrete or lumped parameter models,<sup>5,6</sup> with certain non-linear expressions to represent the forces/torques interactions with the rock formation. These models allow the study of a complex problem by connecting lumped masses, springs, etc, in a conceptually simplified fashion which also facilitate the implementation of control schemes. Yigit and Christoforou<sup>5</sup> developed a lumped parameter model with the scope to analyze the coupled torsional/flexural vibrations of drill-strings. They analyzed qualitatively and quantitatively the vibrations of the drill-string. These authors extended<sup>7</sup> their previous work to include also axial coupling by means of a simplified lumped parameter differential equation in the axial direction. Richard, Germy and Detournay,<sup>6</sup> analyzed the self-excited stick-slip vibrations of drill-strings by means of a simplified lumped parameter model, which accounts for torsional and extensional motions coupled in the boundary. Recently, Trindade, Wolter and Sampaio<sup>4</sup> introduced a non-linear continuous beam model to study the influence of geometrical non-linearities in coupled axial/transversal vibrations of drill-strings. In this work, it was shown that the non-linear model has strong quantitative and qualitative discrepancies with respect to a linear one, and on the other hand an effort was made to show the importance of the use of a continuous model that, by discretization, gives a scheme of approximation; that is, given the error allowed the number of degrees of freedom of discrete model is computed. In the present article, the coupled axial/torsional vibrations of drill-strings are studied by means of a non-linear beam model. The drill-string is subjected to distributed loads due to its own weight, leading to geometrical softening of its lower part due to compression. The finite element method is employed to analyze the vibration patterns of both the non-linear and the linear models in different operative conditions. The linear model can be obtained from the non-linear, neglecting the geometrical stiffening. In this study it is possible to see the qualitative and quantitative differences between linear and non-linear models, especially when the drill-string undergoes stick-slip patterns. These differences are quite remarkable in the calculation of reactive forces and torques. Whereas in linear models there is no geometrical coupling between extensional and torsional vibrations, in the non-linear this kind of geometrical coupling has shown a remarkable effect, specially in long-time stick-slip simulation.

## 2 THEORY FOR THE NON-LINEAR MODEL

### 2.1 Displacements and Strain Measures

Let us consider an initially straight slender beam with annular cross-section ( $R_o$  and  $R_i$  are the outer and inner radii), and of length  $L$  in the undeformed state, which undergoes large displacements and small deformations as shown in the following Figure 1. In this beam model only the coupling between axial and torsional deformations in the dynamics of drill-strings is analyzed. In this context the displacements field vector  $\mathbf{p}$ , of a given point whose coordinates are represented by the vector  $\mathbf{X}$ , is given by:

$$\mathbf{X} = \begin{Bmatrix} x \\ y \\ z \end{Bmatrix} \mapsto \mathbf{p} = \begin{Bmatrix} u(x, t) \\ y(\cos[\theta(x, t)] - 1) - z\sin[\theta(x, t)] \\ y\sin[\theta(x, t)] + z(\cos[\theta(x, t)] - 1) \end{Bmatrix} \quad (1)$$

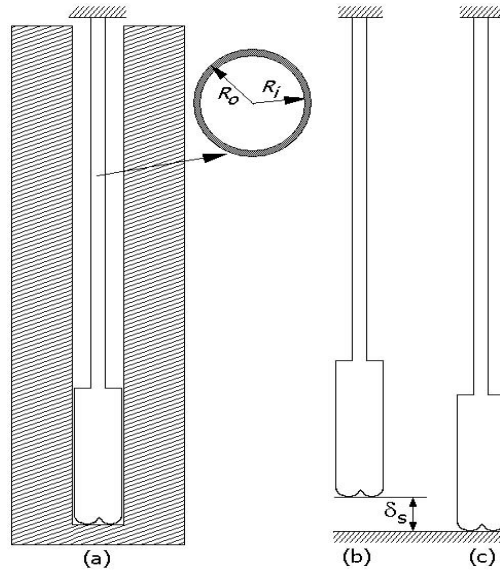


Figure 1: Drill String Scheme. (a) Description (b) Undeformed Configuration (c) Deformed Configuration

the variables  $x$ ,  $y$  and  $z$  are such that  $x \in [0, L]$  and  $\sqrt{y^2 + z^2} \in [R_i, R_o]$ . The Lagrangian strain tensor is described by:

$$\mathbf{E} = \frac{1}{2} \left[ \left( \frac{d\mathbf{p}}{d\mathbf{X}} \right) + \left( \frac{d\mathbf{p}}{d\mathbf{X}} \right)^T + \left( \frac{d\mathbf{p}}{d\mathbf{X}} \right)^T \left( \frac{d\mathbf{p}}{d\mathbf{X}} \right) \right] \quad (2)$$

therefore the components of strain are:

$$\begin{Bmatrix} \epsilon_{xx} \\ \epsilon_{xy} \\ \epsilon_{xz} \end{Bmatrix} = \begin{Bmatrix} \frac{\partial u}{\partial x} + \frac{1}{2} \left[ \left( \frac{\partial u}{\partial x} \right)^2 + \left( \frac{\partial \theta}{\partial x} \right)^2 (y^2 + z^2) \right] \\ -\frac{1}{2} z \frac{\partial \theta}{\partial x} \\ \frac{1}{2} y \frac{\partial \theta}{\partial x} \end{Bmatrix} \quad (3)$$

## 2.2 Variational Formulation

The variational form of the strain energy accounting only for axial and torsional effects can be expressed in terms of strains as follows:

$$\delta H = \frac{1}{2} \delta \int (E\epsilon_{xx}^2 + 4G\epsilon_{xy}^2 + 4G\epsilon_{xz}^2) dV \quad (4)$$

Where  $E$  is the longitudinal modulus of elasticity and  $G$  is the transverse modulus of elasticity. Now, introducing the strain components into the Equation (4), one gets:

$$\delta H = \frac{\delta}{2} \int_0^L [EA(u'^2 + u'^3 + \frac{1}{4}u'^4) + EI_0(u'\theta'^2 + \frac{1}{2}u'^2\theta'^2) + EI_{02}\frac{\theta'^4}{4} + GI_0\theta'^2] dx \quad (5)$$

$A$  and  $I_0$  stand for the cross sectional area and polar moment of inertia, whereas  $I_{02}$  is a generalized cross-sectional constant, defined by:

$$I_{02} = \int_A (y^2 + z^2)^2 dA \quad (6)$$

The variational form of the strain energy can be decomposed in two components, i.e. linear and a non-linear contributions, which can be written as:

$$\delta H = \delta H_L + \delta H_{NL} \quad (7)$$

where

$$\delta H_L = \int_0^L [\delta u' (EA u') + \delta \theta' (GI_0 \theta')] dx \quad (8)$$

$$\delta H_{NL} = \int_0^L \delta u' \left[ \frac{EA}{2} (3u'^2 + u'^3) + \frac{EI_0}{2} (\theta'^2 + u'\theta'^2) \right] dx + \int_0^L \delta \theta' \left[ \frac{EI_0}{2} (2u' + u'^2) \theta' + \frac{EI_{02}}{2} \theta'^3 \right] dx \quad (9)$$

The virtual work done by inertial forces can be written in the following form:

$$\delta T = - \int \rho \delta \mathbf{p}^T \ddot{\mathbf{p}} dV \quad (10)$$

Now, replacing the displacement vector into then above Equation (10), it is possible to obtain:

$$\delta T = - \int_0^L [\delta u (\rho A \ddot{u}) + \delta \theta (\rho I_0 \ddot{\theta})] dx \quad (11)$$

The beam is subjected to its own weight

$$\delta W = \int_0^L \delta u(\rho g A) dx \quad (12)$$

The virtual work of damping is taken into account as a Rayleigh damping proportional to the mass. Then it is possible to write:

$$\delta D = - \int_0^L [\delta u(C_u \dot{u}) + \delta \theta(C_\theta \dot{\theta})] dx \quad (13)$$

where  $C_u$  and  $C_\theta$  are the axial and torsional damping constants calculated from the considerations of Spanos et al.<sup>8</sup>

### 2.3 Non-linear Finite Element Formulation

A Finite Element model can be constructed through discretization of virtual work components of strain, inertia, damping and applied forces. The discretization is carried out using Lagrange linear shape functions for both axial displacements and torsional rotations, that is:

$$\begin{aligned} u &= \mathbf{N}_u \mathbf{q}_e \\ \theta &= \mathbf{N}_\theta \mathbf{q}_e \end{aligned} \quad (14)$$

where defining the element length with  $l_e$ , and the non-dimensional element variable  $\xi = x/l_e$ :

$$\begin{aligned} \mathbf{N}_u &= \{1 - \xi, 0, \xi, 0\} \\ \mathbf{N}_\theta &= \{0, 1 - \xi, 0, \xi\} \\ \mathbf{q}_e^T &= \{u_1, \theta_1, u_2, \theta_2\} \end{aligned} \quad (15)$$

replacing the discrete expressions of displacements into the virtual work expressions, leads to:

$$\begin{aligned} \delta H_L^e &= \delta \mathbf{q}_e^T \mathbf{K}_e^e \mathbf{q}_e \\ \delta H_{NL}^e &= \delta \mathbf{q}_e^T \mathbf{K}_g^e \mathbf{q}_e \\ \delta T^e &= \delta \mathbf{q}_e^T \mathbf{M}^e \ddot{\mathbf{q}}_e \\ \delta D^e &= \delta \mathbf{q}_e^T \mathbf{D}^e \dot{\mathbf{q}}_e \\ \delta W^e &= \delta \mathbf{q}_e^T \mathbf{F}_g^e \end{aligned} \quad (16)$$

where  $\mathbf{K}_e^e$ ,  $\mathbf{K}_g^e$ ,  $\mathbf{M}^e$  and  $\mathbf{D}^e$ , are the elementary matrices of elastic stiffness, geometric stiffness, mass, and damping, respectively, whereas  $\mathbf{F}_g^e$  is the vector of elementary loads due to the gravity field. These matrices and vector are given by the following expressions:

$$\mathbf{K}_e^e = \int_0^1 \left( \frac{EA}{l_e} \mathbf{N}_u'^T \mathbf{N}_u' + \frac{GI_0}{l_e} \mathbf{N}_\theta'^T \mathbf{N}_\theta' \right) d\xi \quad (17)$$

$$\mathbf{K}_g^e = \int_0^1 \left[ \frac{EA}{2l_e^3} (3l_e \mathbf{N}'_u \mathbf{N}'_u \mathbf{q}_e \mathbf{N}'_u + \mathbf{N}'_u \mathbf{N}'_u \mathbf{q}_e \mathbf{q}_e^T \mathbf{N}'_u \mathbf{N}'_u) \right] d\xi + \int_0^1 \left[ \frac{EI_0}{2l_e^3} (l_e \mathbf{N}'_u \mathbf{N}'_\theta \mathbf{q}_e \mathbf{N}'_\theta + \mathbf{N}'_u \mathbf{N}'_u \mathbf{q}_e \mathbf{q}_e^T \mathbf{N}'_\theta \mathbf{N}'_\theta) \right] d\xi + \int_0^1 \left[ \frac{EI_0}{2l_e^3} (2l_e \mathbf{N}'_\theta \mathbf{N}'_u \mathbf{q}_e \mathbf{N}'_\theta + \mathbf{N}'_\theta \mathbf{N}'_\theta \mathbf{q}_e \mathbf{q}_e^T \mathbf{N}'_u \mathbf{N}'_u) \right] d\xi + \int_0^1 \left[ \frac{EI_{02}}{2l_e^3} (\mathbf{N}'_\theta \mathbf{N}'_\theta \mathbf{q}_e \mathbf{q}_e^T \mathbf{N}'_\theta \mathbf{N}'_\theta) \right] d\xi \quad (18)$$

$$\mathbf{M}_e^e = \int_0^1 (\rho A l_e \mathbf{N}'_u \mathbf{N}'_u + \rho I_0 l_e \mathbf{N}'_\theta \mathbf{N}'_\theta) d\xi \quad (19)$$

$$\mathbf{D}_e^e = \int_0^1 (C_u l_e \mathbf{N}'_u \mathbf{N}'_u + C_\theta l_e \mathbf{N}'_\theta \mathbf{N}'_\theta) d\xi \quad (20)$$

The elastic rigidity, inertia, damping and geometric rigidity matrices can be written in the following form:

$$\mathbf{K}_e^e = \begin{bmatrix} \mathbf{A} & -\mathbf{A} \\ -\mathbf{A} & \mathbf{A} \end{bmatrix} \quad \text{with} \quad \mathbf{A} = \frac{1}{l_e} \begin{bmatrix} EA & 0 \\ 0 & GI_0 \end{bmatrix} \quad (21)$$

$$\mathbf{M}_e^e = \begin{bmatrix} 2\mathbf{B} & \mathbf{B} \\ \mathbf{B} & 2\mathbf{B} \end{bmatrix} \quad \text{with} \quad \mathbf{B} = \frac{\rho l_e}{6} \begin{bmatrix} A & 0 \\ 0 & I_0 \end{bmatrix} \quad (22)$$

$$\mathbf{D}_e^e = \begin{bmatrix} 2\mathbf{C} & \mathbf{C} \\ \mathbf{C} & 2\mathbf{C} \end{bmatrix} \quad \text{with} \quad \mathbf{C} = \frac{l_e}{6} \begin{bmatrix} C_u & 0 \\ 0 & C_\theta \end{bmatrix} \quad (23)$$

$$\mathbf{K}_g^e = \frac{EA}{2l_e^3} (3l_e \beta_u + \beta_u^2) \begin{bmatrix} 1 & 0 & -1 & 0 \\ 0 & 0 & 0 & 0 \\ -1 & 0 & 1 & 0 \\ 0 & 0 & 0 & 0 \end{bmatrix} + \frac{EI_{02}}{2l_e^3} \beta_\theta^2 \begin{bmatrix} 0 & 0 & 0 & 0 \\ 0 & 1 & 0 & -1 \\ 0 & 0 & 0 & 0 \\ 0 & -1 & 0 & 1 \end{bmatrix} + \frac{EI_0}{2l_e^2} \begin{bmatrix} 0 & \beta_\theta & 0 & -\beta_\theta \\ \beta_\theta & \beta_u & -\beta_\theta & -\beta_u \\ 0 & -\beta_\theta & 0 & \beta_\theta \\ -\beta_\theta & -\beta_u & \beta_\theta & \beta_u \end{bmatrix} + \frac{EI_0}{2l_e^3} \begin{bmatrix} 0 & \beta_\theta \beta_u & 0 & -\beta_\theta \beta_u \\ \beta_\theta \beta_u & 0 & -\beta_\theta \beta_u & 0 \\ 0 & -\beta_\theta \beta_u & 0 & \beta_\theta \beta_u \\ -\beta_\theta \beta_u & 0 & \beta_\theta \beta_u & 0 \end{bmatrix} \quad (24)$$

where  $\beta_\theta = \theta_2 - \theta_1$  and  $\beta_u = u_2 - u_1$ .

Now, taking into account the virtual work matrix Equation (16) and, operating and assembling in the usual way, one gets the discretized equations of motion:

$$\mathbf{M} \ddot{\mathbf{q}} + \mathbf{D} \dot{\mathbf{q}} + [\mathbf{K}_e + \mathbf{K}_g(\mathbf{q})] \mathbf{q} = \mathbf{F}_g \quad (25)$$

where  $\mathbf{M}$ ,  $\mathbf{D}$ ,  $\mathbf{K}_e$  and  $\mathbf{K}_g$  are the global matrices of mass, damping, elastic stiffness and geometric stiffness, respectively, whereas  $\mathbf{F}_g$  is the global vector of gravity forces. The force vector in the discrete Equation (25) can be extended to account for other force contributions, like impacts, etc.

#### 2.4 Analysis about an initially deformed configuration

In order to analyze the dynamics of the coupled axial/torsional vibrations of the drill-strings, it is important to consider previously some aspects of the drilling process with the scope to characterize the FEM procedure. Drill-strings, such as the ones employed in oil well drilling can be represented by a vertical cylinder with prescribed axial motion at the top position and sliding down due to own weight. When the drill-bit reaches the rock formation, acts a reaction, which is considered time-invariant in this work. At this stage the drill-string starts its rotational motion. Figure 1(b) and Figure 1(c) represent, respectively, the idealized undeformed and deformed configurations of the drill-string. In these circumstances two "a posteriori" forces are included in the finite element model. Then, in addition to the gravity force vector  $\mathbf{F}_g$  present in Equation (25), in the bottom node is applied a time-independent force  $\mathbf{F}_f$  to simulate the axial reaction due to rock formation. In addition a reactive torque  $T_{bit}$  is applied through the external generalized force vector  $\mathbf{F}_T$ . This reactive torque is applied at the bottom node N, i.e. in the  $(2N)^{th}$  degree of freedom, and it can be modeled combining different interaction models (for example: Kreuzer and Kust,<sup>9</sup> and Yigit and Christoforou<sup>7</sup>), in the following form:

$$T_{bit} = \mathbf{F}_{T_{2N}} = \mu W_{ob} f_i(\theta_{bn}) \left[ \text{Tanh}[\dot{\theta}_{bn}] + \frac{\alpha_1 \dot{\theta}_{bn}}{1 + \alpha_2 \dot{\theta}_{bn}^2} \right] \text{ with} \quad (26)$$

$$f_i(\theta_{bn}) = \begin{cases} f_1(\theta_{bn}) = \frac{1}{2} (1 + \text{Cos}[\theta_{bn}]) \\ f_2(\theta_{bn}) = 1 \end{cases}$$

where  $W_{ob}$  is the axial reaction of the rock formation,  $\mu$  is a factor depending on the drill cutter characteristics,  $\alpha_1$  and  $\alpha_2$  are constants depending on rock properties,  $f_i(\theta_{bn})$  is introduced to exploit different modeling options and  $\theta_{bn}$  and  $\dot{\theta}_{bn}$  are the rotational angle and speed at the drill bit respectively.

Therefore, considering the aforementioned background, Equation (25) can be rewritten in the following form:

$$\mathbf{M} \ddot{\mathbf{q}} + \mathbf{D} \dot{\mathbf{q}} + [\mathbf{K}_e + \mathbf{K}_g(\mathbf{q})] \mathbf{q} = \mathbf{F}_g + \mathbf{F}_f + \mathbf{F}_T \quad (27)$$

In this work, it is supposed that after the quasi-static lowering and when the reaction force reaches a prescribed value the axial displacement of the drill bit is locked as it is suggested in

Figure 1(c). Then further motions take place around this initial deformed configuration, which is obtained from the following equation:

$$\mathbf{q}_s = \mathbf{K}_e^{-1} (\mathbf{F}_g + \mathbf{F}_f) \quad (28)$$

It has to be pointed out that Equation (28) was obtained assuming that the geometric stiffness is negligible compared to the elastic stiffness for the initial axial loading, as it was explained in Trindade, Wolter and Sampaio.<sup>4</sup> Then, defining a new displacement vector  $\bar{\mathbf{q}}$  relative to the static  $\mathbf{q}_s$ , as

$$\bar{\mathbf{q}} = \mathbf{q} - \mathbf{q}_s \quad (29)$$

substituting  $\mathbf{q}$  from Equation (29) into Equation (25) and taking into account Equation (25), it is possible to obtain the following equations of motion (30) in terms of  $\bar{\mathbf{q}}$ , i.e in terms of the relative displacement vector:

$$\mathbf{M} \ddot{\bar{\mathbf{q}}} + \mathbf{D} \dot{\bar{\mathbf{q}}} + [\mathbf{K}_e + \mathbf{K}_g (\bar{\mathbf{q}} + \mathbf{q}_s)] \bar{\mathbf{q}} = \mathbf{F}_T \quad (30)$$

Then, the axial displacement of the drill bit it locked into its static value, that is:  $\bar{u}^L = 0$  or  $u = u_s^L$ . On the other hand the top position of the drill-string is subjected to a constant rotary speed  $\omega$ .

### 3 NUMERICAL RESULTS AND ANALYSIS

In the present section, the dynamics of typical drill string configuration is simulated in order to identify the influence of the geometric axial/torsional coupling. The geometrical and material properties of drill string are those presented in Table 1. The drill string consists of two parts, the upper portion is composed of slender drill pipes normally subjected to large traction forces; on the other hand, the lower portion is subjected to compressive forces due to the action of own weight of the upper part and the reactive forces, consequently the lower part has larger diameters.

Table 1: Geometrical and Material properties of the drill string

Property	Section 1	Section 2
Longitudinal Elastic Modulus $E$ (GPa)	210	210
Transversal Elastic Modulus $G$ (GPa)	80	80
Mass density $\rho$ (kg/m <sup>3</sup> )	7850	7850
Internal Diameter (m)	0.09718	0.05715
External Diameter (m)	0.11430	0.16510 <sup>868</sup>
Length (m)	2250	250

Since in the present study the axial displacements are supposed to be initially at their static configuration, they can be excited by means of the coupling with the torsional vibrations. In these circumstances while the rock reaction is supposed constant (the drill string is lowered until it reaches a prescribed value), the only axial/torsional structural-interaction comes from the non-linear strain-displacement relations, not present in the linear model. The family of Matlab ode-solvers was employed to obtain numerical approximations of the solution, for this reason (30) has to be written as a first order equation.

### 3.1 Convergence Studies

In this section a convergence study is carried out. The Matlab solver ode15s was employed to integrate the discretized equation. A relative tolerance error of  $\epsilon_r = 10^{-8}$  was adopted in the solver. The rock-bit interaction parameters  $\alpha_1 = \alpha_2 = 1$  are employed in Equation (26). The drill-bit parameter has the value  $\mu = 0.04$ . The drill-string is subjected to a prescribed rotary speed of 10 rad/seg at the top. The torque was modeled with function  $f_i(\theta_{bn}) = f_1(\theta_{bn})$ , that is the form varying with the rotation angle.

A measure of convergence can be obtained by means of the relative error (between a coarse and the finest discretizations) calculated by expressions (31) and (32) for angular velocity and rotation angles, respectively. These expressions are computed in a given point  $x_g$  and at given integration instant  $t_g$ .

$$e\% = 100 \left| \frac{\dot{\theta}(x_g, t_g)_{coarse} - \dot{\theta}(x_g, t_g)_{finest}}{\dot{\theta}(x_g, t_g)_{finest}} \right| \quad (31)$$

$$e\% = 100 \left| \frac{\theta(x_g, t_g)_{coarse} - \theta(x_g, t_g)_{finest}}{\theta(x_g, t_g)_{finest}} \right| \quad (32)$$

Figure 2(a) shows a convergence of the angular velocity in the drill-bit calculated at instants  $t_g = 5$  sec. and  $t_g = 15$  sec. for models with different number of elements. Figure 2(b) shows the relative error for the rotation angle in the drill-bit at the same instants.

In Figure 2(b), one observes a fast convergence of the rotation angle measured at the instant  $t_g = 15$  sec in comparison to the case measured at instant  $t_g = 5$  sec. This is reasonable due to the fact that as the drill-bit evolves the rotation angle becomes larger, whose effect is to reduce the relative error (see for example Figure 3(a) for a measure of the magnitude of rotation angle). Consequently, coarser models reach acceptable convergence for the rotation angle. However, in practical drilling process there is more interest in the behavior of angular velocity than rotation angles. Now, in Figure 2(a), it is possible to see a slow convergence of angular velocity for the coarser models (10 and 18 elements) at the beginning instants (i.e.  $t_g = 5$  sec). Models with more than 22 elements give better responses and a faster convergence for  $t_g = 5$  sec. But, to reach a good convergence at instant  $t_g = 15$  sec one needs discretizations with more than 18 elements, and to reach reasonable convergence at instants  $t_g \geq 15$  sec. it is imperative to employ the finest mesh possible. However, the use of finer meshes demands greater computational

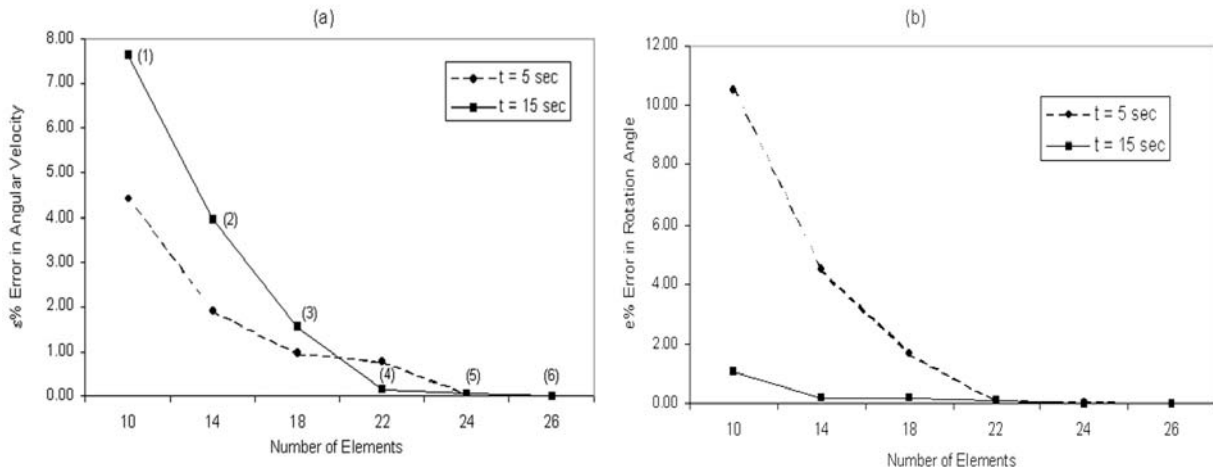


Figure 2: Convergence of approximation at drill-bit (a) angular velocity (b) rotation angle

effort. In other word, the total calculation time required for the model at points (1) and (3) in Figure 2(a) were 420 and 660 seconds, respectively; however the calculation time required at points (4), (5) and (6) in the same Figure were 1100, 3220 and 8900 seconds, respectively. The calculations were carried out on a Pentium M (1.7 GHz) with RAM of 1.0 Gb.

### 3.2 Comparison of Matlab solvers

As it was mentioned in the previous subsection the integration was carried out employing the Matlab solver ode15s, which is an implicit solver for "stiff" systems. However, with the aim to evaluate the efficiency and performance of other solvers available in Matlab, a comparison between implicit and explicit solvers is presented in this section. Models with 22 elements were tested employing two implicit solvers for "stiff systems" (ode15s and ode23s) and other two for "non-stiff systems" (ode113 and ode45). Figure 3(a) shows the variation of the drill-bit angular rotation calculated with the four solvers with a relative error tolerance of  $\epsilon_r = 10^{-8}$ . Figure 3(b) shows the difference of the responses of ode45, ode113 and ode23s with respect to ode15s. Figure 4 shows the same results but for the rotation velocity (where  $\partial_t \theta(t)$  means the rotary speed, i.e derivation with respect to the time). The absolute error of solver-responses presented in Figures 3(b) and 4(b) are calculated with expressions (33) and (34) respectively.

$$\epsilon_{\theta} = \theta(x_g, t)_{odeXX} - \theta(x_g, t)_{ode15s} \quad (33)$$

$$\epsilon_{\dot{\theta}} = \dot{\theta}(x_g, t)_{odeXX} - \dot{\theta}(x_g, t)_{ode15s} \quad (34)$$

One observes that although in Figures 3(b) and 4(b) there are absolute differences between two solvers, the relative errors are insignificant in relation to the values of the rotation angle and angular velocity.

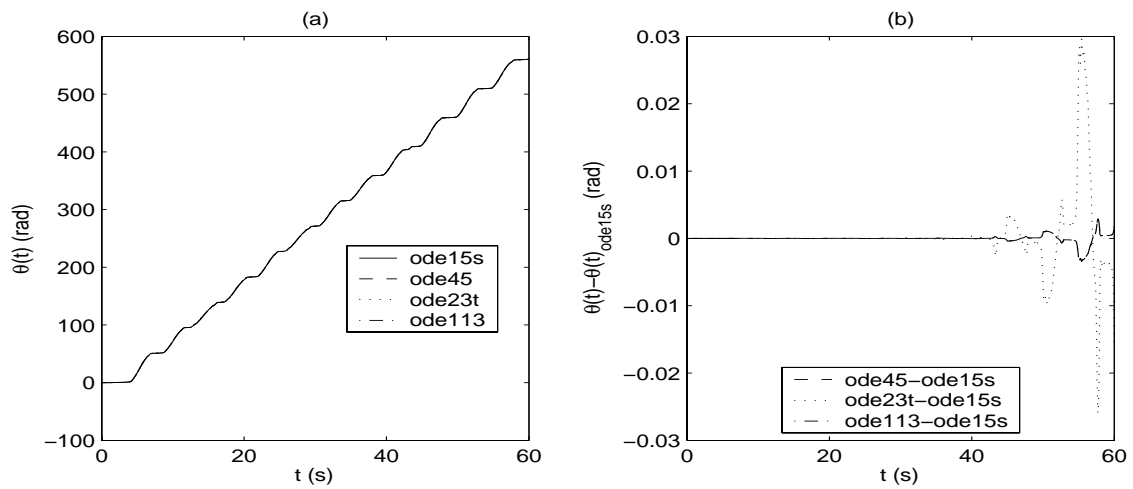


Figure 3: Performance of Matlab Solvers (a) rotation angle at drill-bit (b) difference with respect to ode15s

Table 2: Computing-cost (in seconds) of Matlab solvers for different prescribed relative error tolerances

Solver	$\epsilon_r = 10^{-8}$	$\epsilon_r = 10^{-12}$
ode15s	1692	6956
ode23s	7123	27456
ode113	359	1508
ode45	1270	4953

The Table 2 presents the time demanded for each solver to calculate the response of a 60 seconds period, for different cases of internal error tolerance adopted in the ode solvers. One can see huge amount of time demanded to obtain the response for internal error tolerance of  $\epsilon_r = 10^{-12}$  instead of  $\epsilon_r = 10^{-8}$ . As it can be inferred the selection of a particular solver involves the decision of the computing cost which, for this problem may vary between few minutes and more than seven hours.

The selection of Matlab solvers instead of the Newmark’s family of solvers to integrate the discrete equations has two connected reasons. The first reason is related to the numerical performance of the Newmark’s method, which depends on the selection of certain parameters that can lead to an unstable numerical behavior. Although, it is possible to add numerical damping with the scope to stabilize the method, not always this alternative gives good results. The second reason is connected with the fact that for strong non-linear problems (specially when the excitation force directly depends on the speed and displacement) the time-step has to be smaller, consequently demanding more computational effort. The authors also have carried out a calculation -not shown here- with the Newmark’s Method (with 20 finite element, parameters  $\gamma = 0.5$  and  $\beta = 0.25$ ) for the problem studied in this section, that demanded more than twelve

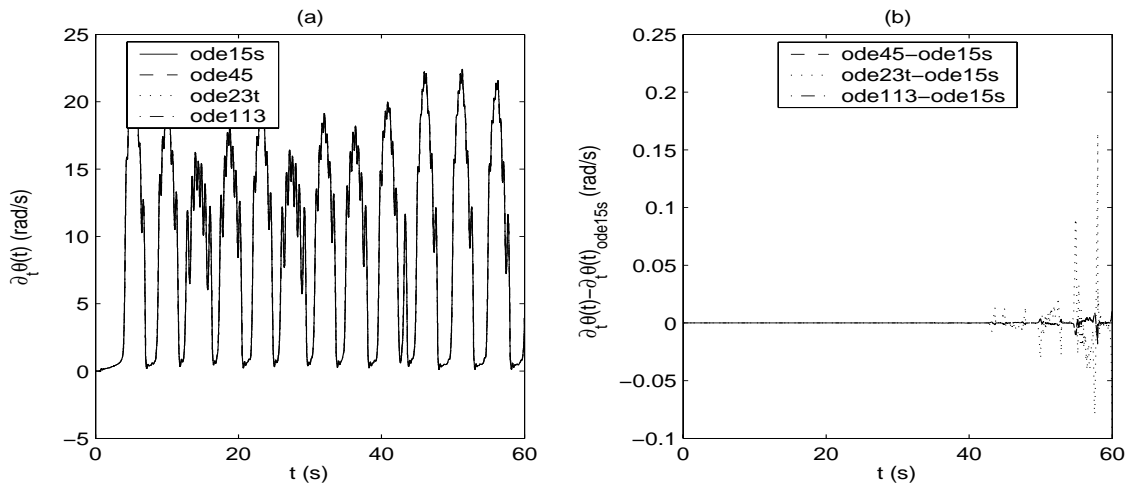


Figure 4: Performance of Matlab Solvers (a) angular velocity at drill-bit (b) difference with respect to ode15s

hours to calculate a period of thirty seconds without numerical instabilities.

### 3.3 Comparison of Torque Modeling

The Equation (26) offers two alternatives to model the perturbation torque. Kreuzer and Kust<sup>9</sup> employed a form which depends on the rotation angle and the rotary speed at the drill-bit, other authors such as Yigit and Christoforou<sup>5</sup> among others employed a torque on bit which only depends on the rotary speed at the drill-bit. The ode15s solver was used to integrate a model with 22 finite elements.

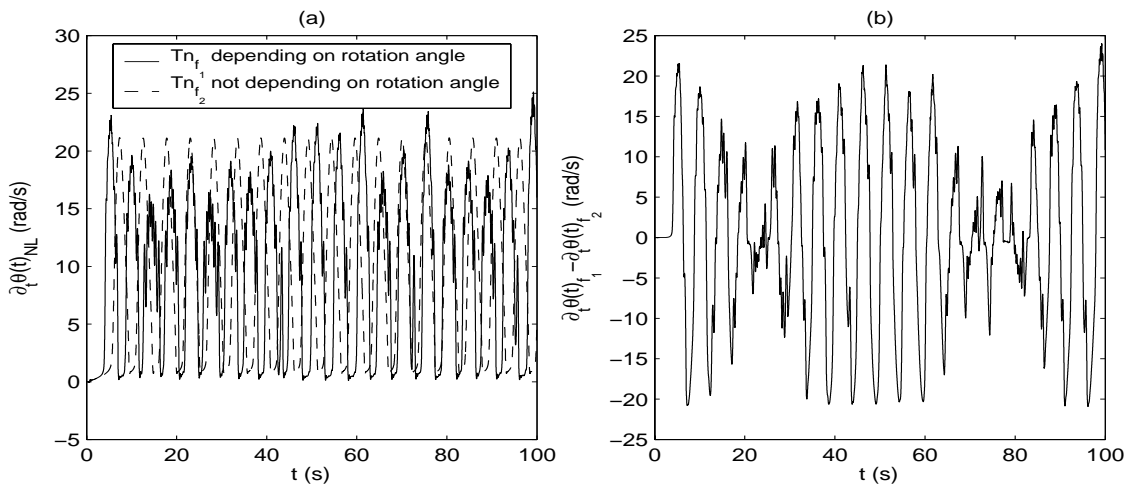


Figure 5: Effect of perturbation torques (a) angular velocity at drill-bit (b) difference of responses

Figure 5(a) shows the angular velocity at the drill-bit for both perturbation torques defined in (26). Figure 5(b) offers the absolute difference between the angular velocity due to both torques, i.e.  $\dot{\theta}(t, T_{n_{f_1}(\theta_{bn})}) - \dot{\theta}(t, T_{n_{f_2}(\theta_{bn})})$ . The stick-slip pattern is obviously modified. The use of  $f_i(\theta_{bn}) = f_2(\theta_{bn})$  instead of  $f_i(\theta_{bn}) = f_1(\theta_{bn})$  in equation (26), leads to a reduction of the quantity of stick-slip periods, giving uniform angular velocity peaks.

### 3.4 Simulation and Analysis of Stick-Slip Behavior

In order to understand the stiffening/softening effects and axial/torsional interactions in the drilling process, a set of comparisons between linear and non-linear models are performed. The following rock-bit interaction parameters  $\alpha_1 = \alpha_2 = 1$  and  $f_i(\theta_{bn}) = f_1(\theta_{bn})$  are employed in Equation (26). The drill-bit parameter can have the values  $\mu = 0.04$  or  $\mu = 0.06$ . The drill-string is subjected to a forcing rotary speed of 10 rad/seg at the top. The drill-string was modeled with 22 finite elements (3 in the lower segment and 19 in the upper segment), and as explained in the previous section, the axial displacement of the drill bit is locked when a reactive axial force of  $2.55 \times 10^5$  N due to the rock formation is reached. The equations of motion (30) for the discretized equations were numerically integrated with the aid of Matlab ODE algorithms based on implicit schemes (ode15s).

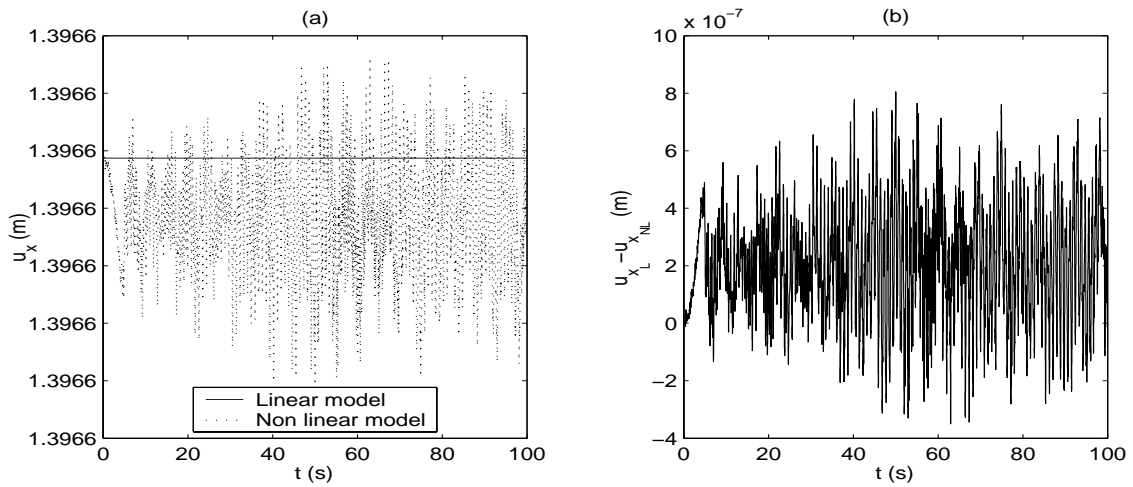


Figure 6: Axial displacement at  $u_{2490}$  m from the top position (a) Comparison of models (b) Difference of models

Figure 6 shows the axial displacement at a point 10 m from the bottom (that is  $u_{2490}$ ), for both linear and non-linear models. It is possible to see that the axial displacement in the linear model do not vary with respect to the time (Figure 6(a)). This is due to the fact, that in the linear model the axial displacement is not coupled with the rotational degree of freedom (which is the only one perturbed via the generalized force vector  $\mathbf{F}_T$ ) and due to the fact that the axial reaction is assumed constant in this study. On the other hand it is possible to see that in the non-linear model, the axial displacement is indeed perturbed by the rotational degree of freedom. The

effect of the variation of axial displacement of the non-linear model with respect to the linear is smaller as it is possible to see in Figure 6(b) (which shows the difference of both responses), and that is why it is normally neglected in static analysis. However this effect can be qualitatively appreciated in the calculation of forces, which will be showed in the next paragraphs.

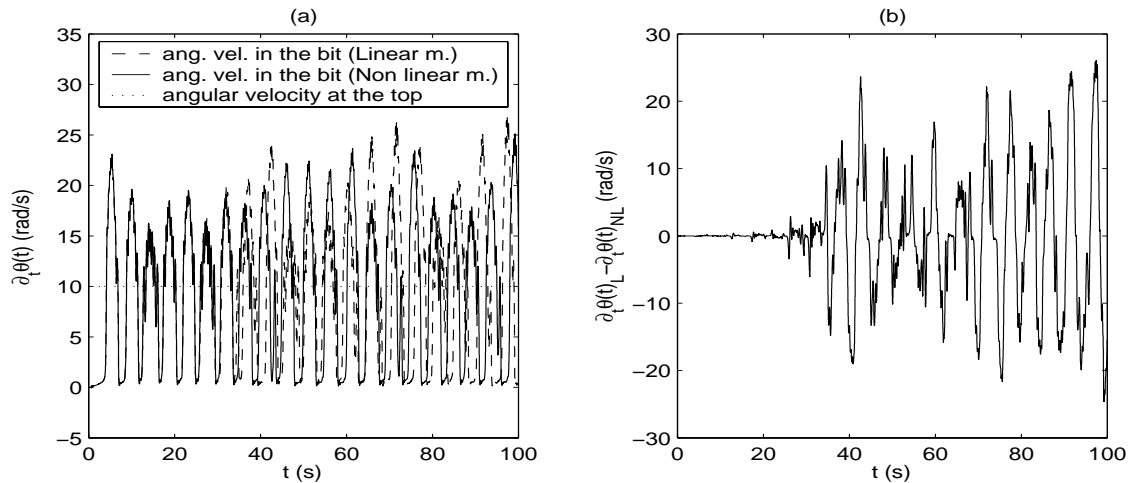


Figure 7: Difference of non-linear and linear responses in the angular speed at bit, for the case of  $\mu = 0.04$

Figure 7(a) depicts the rotary speed at bottom position for both models with drill parameter  $\mu = 0.04$  (in the Figures  $\partial_t \theta(t)$  means the rotary speed, whereas sub indexes L and NL correspond to linear and non-linear models, respectively). The forcing rotary speed at the top position is also depicted for comparison purposes. In Figure 7(b) is possible to see a divergence of both models, characterized by the difference between their corresponding rotary speeds. This difference starts to be sensible after the first 30 seconds of the evolution. The following Figures 8(a) and 8(b) show the homonymous information of the previous Figures 7(a) and 7(b) but with drill parameter  $\mu = 0.06$ . In this case the divergence of linear and non-linear models commences being evident after the first 25 seconds of evolution. In Figs. 7(a) and 8(a), the vibration pattern of linear and non-linear models corresponds to a stick-slip situation. In these circumstances the linear model predicts higher peaks of rotary speed that the non-linear model. The rotary speed at the drill-bit shows peaks which can reach more than twice the value of forcing rotary speed at the top position. Also the increase of factor  $\mu$  leads to an increase in the level of speed peaks, as seen in Fig. 7(a) and Fig. 8(a).

In Figure 9 the axial reaction at the top position for both linear and non-linear models is shown. In this Figure is possible to see that the qualitative differences of both models are sensible. In fact the employment of a non-linear model leads to an modification in the axial force behavior due to torsional vibration. In other words, the presence of torsional displacements geometrically coupled to axial displacements, induce an increase of the last ones, leading to an qualitative variation of the axial deformation.

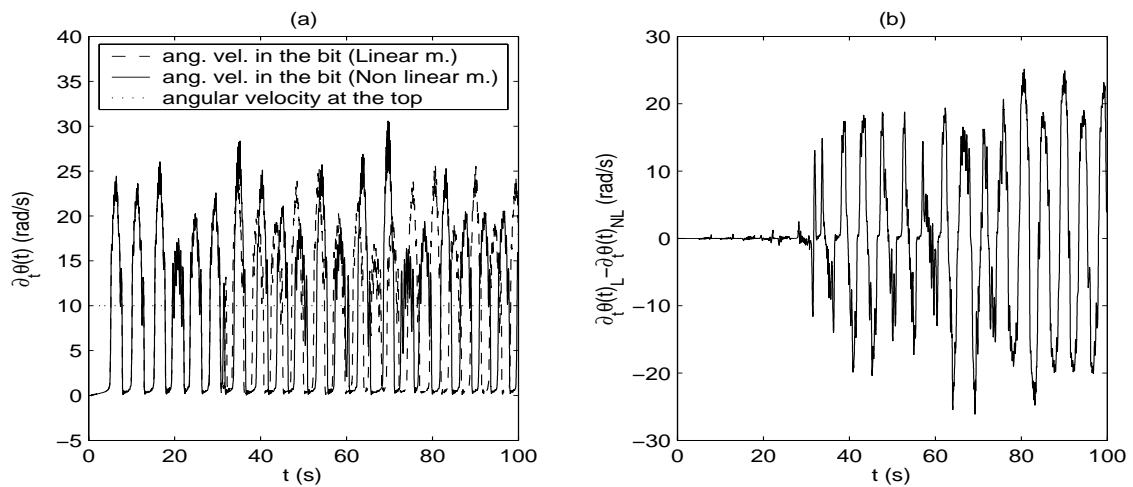


Figure 8: Difference of non-linear and linear responses in the angular speed at bit, for the case of  $\mu = 0.06$

#### 4 CONCLUSIONS

In this article a non-linear model for simulation of the axial/torsional interactions in drill-strings dynamics was introduced. Other aspect of this article was the qualitative study about integration schemes in order to characterize and identify the features that facilitate the analysis of the non-linear model developed. Four ode solvers of Matlab were tested. These results suggest that for the case of extensional/torsional vibrations of drill-strings the use of a particular integration method may lead to a sensible spare of time preserving the accuracy of the numerical approximation. The use of Matlab solvers can offer a good alternative to well known solvers of Newmark's family methods which can have numerical instabilities and requires a lot of computing effort. The effect of torque modeling was also analyzed. The perturbation torque depending only on the angular velocity (i.e. with  $f_i(\theta_{bn}) = f_2(\theta_{bn})$ ) has the effect to reduce the quantity of stick-slip periods in the drill-bit. The axial/torsional interactions were analyzed by means of a comparison between the responses of linear and non-linear models, in operative conditions. Normally, the axial/torsional interaction of a linear model is only related to the bit torque, which has a non-linear form depending on rotation speed and rotation angle at the bit. However, the non-linear model has, in addition to the non-linear bit torque, the consideration of a geometric coupling due to non-linear strain-displacements relations. As was stated in the previous paragraphs, the introduced non-linear beam model can be reduced to a linear one leaving out the non-linear strain-displacements effects. The linear and non-linear models differ considerably after the first periods of stick-slip not only in the drill-bit rotary speed. Also the linear and non-linear models differ qualitatively in the calculation of forces and torques in general, but particularly for the reactive axial forces. This observation is crucial in order to simulate a long-time analysis of drilling process, as well as to consider some control methodologies. However the consideration of control methodologies based on the present model is the matter for future

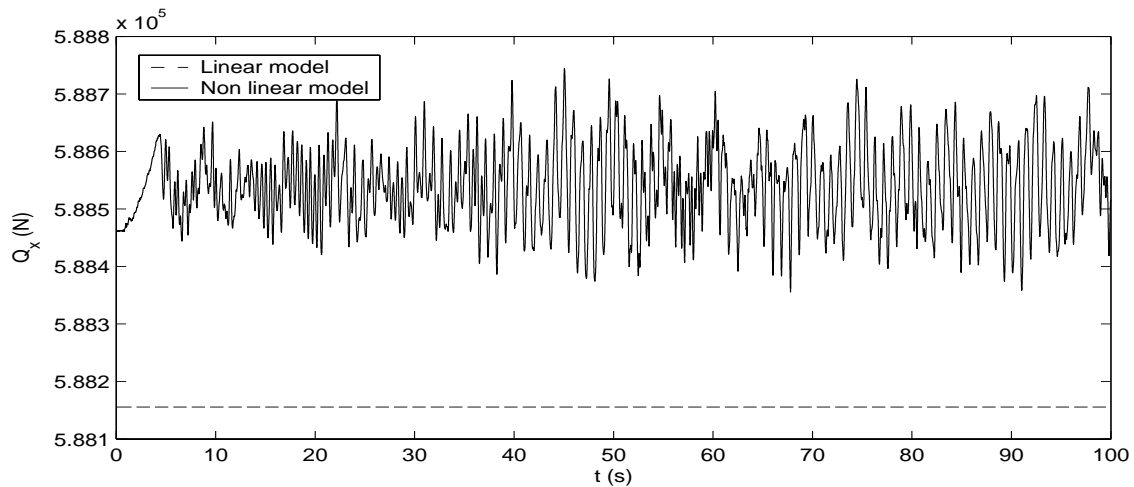


Figure 9: Reaction forces at the top position using linear and non-linear models

research.

## 5 ACKNOWLEDGEMENTS

This work was supported by CNPq, Project 470814/2003-9. The second author also thanks the Grant 2004-1368 of Organización de los Estados Americanos (OEA), and the support of Universidad Tecnológica Nacional, Facultad Regional Bahía Blanca.

## REFERENCES

- [1] I. Sharf. Geometric stiffening in multibody dynamics formulations. *Journal of Guidance, Control and Dynamics*, **18**(4), 882–890 (1995).
- [2] A.K. Banerjee and J.M. Dickens. Dynamics of an arbitrary flexible body in large rotation and translation. *Journal of Guidance, Control and Dynamics*, **13**(2), 221–227 (1990).
- [3] M.A. Trindade and R. Sampaio. Dynamics of beams undergoing large rotations accounting for arbitrary axial rotations. *Journal of Guidance, Control and Dynamics*, **25**(4), 634–643 (2002).
- [4] M.A. Trindade, C. Wolter, and R. Sampaio. Karhunen-loève decomposition of coupled axial/bending vibrations of beams subjected to impact. *Journal of Sound and Vibration*, **279**, 1015–1036 (2005).
- [5] A.S. Yigit and P. Christoforou. Coupled torsional and bending vibrations of actively controlled drillstrings. *Journal of Sound and Vibration*, **234**(1), 67–83 (2000).
- [6] T. Richard, C. Germy, and E. Detournay. Self-excited stick-slip oscillations of drill bits. *Comptes Rendus Mecanique*, **332**, 619–626 (2004).
- [7] A.S. Yigit and P. Christoforou. Fully coupled vibrations of actively controlled drillstrings. *Journal of Sound and Vibration*, **267**, 1029–1045 (2003).

- [8] P.D. Spanos, A.K. Sengupta, R.A. Cunningham, and P.R. Paslay. Modelling of roller cone bit lift-off dynamics in rotary drilling. *Journal of Energy Resources Technology*, **117**, 197–207 (1995).
- [9] E. Kreuzer and O. Kust. Analysis of torsional strings by proper orthogonal decomposition. *Archive of Applied Mechanics*, **67**, 68–80 (1996).